Journal of Power Sources 250 (2014) 152–159

Contents lists available at ScienceDirect

Journal of Power Sources

journal homepage: www.elsevier.com/locate/jpowsour

A modified liquid-phase-assisted sintering mechanism for $La_{0.8}Sr_{0.2}Cr_{1-x}Fe_xO_{3-\delta}$—A high density, redox-stable perovskite interconnect for solid oxide fuel cells

Tao Wei [a], Xiaojuan Liu [a], Chun Yuan [b], Qingyu Gao [a], Xianshuang Xin [b], Shaorong Wang [a,b,*]

[a] College of Chemistry and Chemical Engineering, China University of Mining and Technology, Xuzhou 221116, China
[b] CAS Key Laboratory of Materials for Energy Conversion, Shanghai Institute of Ceramics, Chinese Academy of Sciences, 1295 Dingxi Road, Shanghai 200050, China

HIGHLIGHTS

- A modified liquid-phase-assisted sintering mechanism is employed.
- A distinct transient liquid phase forms during the sintering process.
- Relative density of 96.6% is successfully obtained for La0.8Sr0.2Cr0.5Fe0.5$O_{3-\delta}$.
- La0.8Sr0.2Cr0.5Fe0.5$O_{3-\delta}$ is proposed as a promising interconnect for SOFCs.

GRAPHICAL ABSTRACT

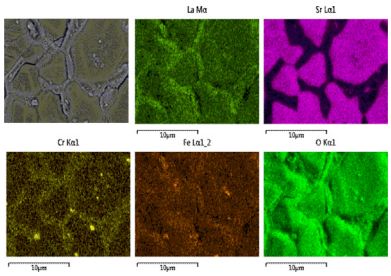

ARTICLE INFO

Article history:
Received 3 August 2013
Received in revised form
9 November 2013
Accepted 11 November 2013
Available online 20 November 2013

Keywords:
SOFCs
Redox-stable
Interconnect
Perovskite
Liquid phase

ABSTRACT

Fe-doped lanthanum strontium chromites, i.e., $La_{0.8}Sr_{0.2}Cr_{1-x}Fe_xO_{3-\delta}$ (x = 0.1, 0.2, 0.3, 0.4, and 0.5), are synthesised and evaluated as potential interconnect materials for SOFCs. A modified liquid-phase-assisted sintering mechanism is employed to improve the sintering abilities of $La_{0.8}Sr_{0.2}Cr_{1-x}Fe_xO_{3-\delta}$ powders. A distinct transient liquid phase forms during the sintering process, which spreads into a uniform layer and covers the grain boundaries, thereby enhancing densification. Additionally, it is determined that the amount of liquid phase formed during liquid-phase-assisted sintering significantly affects the densification of doped lanthanum chromites. Relative densities of 94.6% and 96.6% are successfully obtained for $La_{0.8}Sr_{0.2}Cr_{0.6}Fe_{0.4}O_{3-\delta}$ and $La_{0.8}Sr_{0.2}Cr_{0.5}Fe_{0.5}O_{3-\delta}$, respectively. Furthermore, these compounds are also redox-stable after being heated to 900 °C in flowing H_2 for 6 h. The electrical conductivity increases with Fe-doping levels, and the conductivity of $La_{0.8}Sr_{0.2}Cr_{0.5}Fe_{0.5}O_{3-\delta}$ is measured to be 21.88 S cm^{-1} in air and 6.45 S cm^{-1} in 5% H_2/Ar at 800 °C. Therefore, dense $La_{0.8}Sr_{0.2}Cr_{0.5}Fe_{0.5}O_{3-\delta}$ is a promising interconnect alternative for solid oxide fuel cells.

1. Introduction

Solid oxide fuel cells (SOFCs) have attracted considerable interest as a new, clean power generation system with high efficiency. The fuel flexibility of SOFCs makes them an ideal candidate for the effective use of fossil fuels [1–3]. Tubular and planar stack designs are currently the two main SOFC concepts being developed. Tubular SOFCs have certain advantages over planar SOFCs, including ease of sealing and the ability to endure thermal stress caused by rapid heating [4–6]. Unfortunately, only ceramic interconnects can be used in tubular SOFCs [7]. The interconnect, which provides the conductive path for electrical current and separates the fuel gas

* Corresponding author. Tel./fax: +86 21 52411520.
E-mail addresses: srwang@mail.sic.ac.cn, 515755699@qq.com (S. Wang).

0378-7753/$ – see front matter © 2013 Elsevier B.V. All rights reserved.
http://dx.doi.org/10.1016/j.jpowsour.2013.11.012

from the oxidant, is an essential part of the SOFC stack. Therefore, the interconnect should be dense, sufficiently conductive, and stable in both oxidising and reducing atmospheres under high temperatures. Because of these strict requirements, only a few materials can be used for SOFC interconnects. $LaCrO_3$-based perovskites, which exhibit high thermal and chemical stability in dual oxidation–reduction atmospheres and good electrical conductivity, are the most promising materials [8–10]. However, the poor sinterability of these compounds in air, because of increased rates of chromium evaporation, imposes a major constraint to their fabrication and utility. Various methods have been suggested to improve the sinterability of doped lanthanum chromite powders, including adding sintering aids [11,12], sintering in a reducing atmosphere [13], using chromium deficient non-stoichiometric composition [14,15], and substituting lanthanum with other elements [12,16]. Nevertheless, adding sintering aids and sintering in a reducing atmosphere increases fabrication complexity and manufacturing costs, whereas using a chromium deficient non-stoichiometric composition causes compositional inhomogeneity. It was determined that the presence of low-melting Ca-rich secondary phases, such as $CaCrO_4$ or $Ca_n(CrO_3)_m$, support the sintering of $La(Ca)CrO_3$ by a liquid-phase-assisted sintering mechanism. However, excess A-site elements tend to react with the zirconia electrolyte during sintering, which produces undesirable secondary phases, such as $La_2Zr_2O_7$ and $CaZrO_3$ [17,18]. Moreover, heavy Ca-doping reduces the chemical and dimensional stability in reducing environments, which decomposes the perovskite structure in fuel conditions [19]. Additionally, chemical expansion causes internal stress and deformation under large oxygen partial pressure gradients [20]. Therefore, an alternative interconnect material is required to overcome the technical limitations of acceptor-doped lanthanum chromite.

To the best of our knowledge, there have been few investigations on aliovalent cation doping of B (Cr) sites for interconnect development. Thus, we hypothesise that doping the B-site with large cations will enhance the diffusion of larger A-site cations during the sintering process. Additionally, doping on the B-site could enhance other properties that may resolve the problems that were previously mentioned [21]. For example, Tao and co-authors [22] have reported that $La_{0.75}Sr_{0.25}Cr_{1-x}Fe_xO_3$ with $x \leq 0.5$ is stable in dry 5% H_2 at 900 °C. Liu et al. [23] successfully prepared $Zr_{0.84}Y_{0.16}O_{1.92}$ (YSZ) and $La_{0.8}Sr_{0.2}Cr_{0.5}Fe_{0.5}O_{3-\delta}$ (LSCF) dual-phase composite hollow fibres for oxygen permeation membranes in which oxide ions were transported through YSZ and electrons were transported through LSCF. Furthermore, the ionic conductivity of $(La_{0.75}Sr_{0.25})_{0.95}Cr_{0.6}Fe_{0.4}O_{3-\delta}$ was determined to be 0.079 S cm^{-1} at 1223 K with $p(O_2) = 10^{-17}$ atm [24], which is smaller than the ionic conductivity of YSZ (0.1 S cm^{-1}) [1]. Based on these results, and if it has a sufficient density (the accepted density for a ceramic interconnect is 94% [25,26]), Fe-doped lanthanum strontium chromite is expected to satisfy the requirements for use in SOFC interconnects.

In the present work, $La_{0.8}Sr_{0.2}Cr_{1-x}Fe_xO_{3-\delta}$ ($x = 0.1$, 0.2, 0.3, 0.4, and 0.5) was synthesised and characterised. Relative densities of 94.6% and 96.6% were successfully obtained by a modified liquid-phase-assisted sintering mechanism for $La_{0.8}Sr_{0.2}Cr_{0.6}Fe_{0.4}O_{3-\delta}$ and $La_{0.8}Sr_{0.2}Cr_{0.5}Fe_{0.5}O_{3-\delta}$, respectively. The microstructure, electrical conductivities, thermal expansion coefficients, and other properties of $La_{0.8}Sr_{0.2}Cr_{1-x}Fe_xO_{3-\delta}$ were also investigated. An optimised composition for use in a SOFC interconnect is proposed. The oxygen nonstoichiometry (δ) of $La_{0.8}Sr_{0.2}Cr_{1-x}Fe_xO_{3-\delta}$ is important because it is closely correlated to the electrochemical properties, mechanical properties, and stability of the material. However, in the present work, we focused on the densification of $La_{0.8}Sr_{0.2}Cr_{1-x}Fe_xO_{3-\delta}$, which is an extremely critical parameter for the interconnect. The effect of δ will be investigated in future studies.

2. Experimental section

All $La_{0.8}Sr_{0.2}Cr_{1-x}Fe_xO_{3-\delta}$ ($x = 0.1$, 0.2, 0.3, 0.4, 0.5) specimens were synthesised individually using the sol–gel method. Metal ion nitrate solutions were prepared from La_2O_3, $SrCO_3$, $Fe(NO_3)_3\cdot 9H_2O$ and $Cr(NO_3)_3\cdot 9H_2O$. First, La_2O_3 and $SrCO_3$ were dissolved in diluted nitric acid, and $Fe(NO_3)_3\cdot 9H_2O$ and $Cr(NO_3)_3\cdot 9H_2O$ were dissolved in de-ionised separately in water. Next, the metal nitrate solutions were mixed together in a proper ratio. An excess of citric acid was added, and the pH of the solution was carefully adjusted to the required level with NH_4OH. The mixtures were placed in a water bath at 80 °C with constant stirring for approximately 3 h to evaporate excess water and obtain a gel. The as-prepared gel was dried at 200 °C and calcined in a temperature range from 900 to 1200 °C for 4 h in air. The crystal structures of the synthesised powder specimens were determined by X-ray diffraction (XRD) with Cu Kα radiation (D8 Advance, Bruker AXS, Germany; 40 kV, 30 mA) at room temperature. To estimate the lattice parameters, the measured XRD patterns were refined using Rietveld refinement. The morphology of the sintered samples was characterised with a field emission scanning electron microscope (S-4800, Hitachi, Japan). Thermal expansion coefficients (TECs) were determined using a TMA 402 F1 Hyperion (Netzsch, Germany).

For the purpose of convenience, $La_{0.8}Sr_{0.2}Cr_{0.9}Fe_{0.1}O_{3-\delta}$, $La_{0.8}Sr_{0.2}Cr_{0.8}Fe_{0.2}O_{3-\delta}$, $La_{0.8}Sr_{0.2}Cr_{0.7}Fe_{0.3}O_{3-\delta}$, $La_{0.8}Sr_{0.2}Cr_{0.6}Fe_{0.4}O_{3-\delta}$ and $La_{0.8}Sr_{0.2}Cr_{0.5}Fe_{0.5}O_{3-\delta}$ are abbreviated as Fe 0.1, Fe 0.2, Fe 0.3, Fe 0.4 and Fe 0.5, respectively, throughout this paper.

3. Results and discussion

3.1. Crystal structure

The XRD patterns taken at room temperature of Fe 0.5 powders calcined at 900, 1000, 1100, 1200 °C are shown in Fig. 1. The Fe 0.5 specimens are shown as representative results; the other compositions exhibited similar characteristics. The XRD patterns reveal that although the samples were calcined at different temperatures they all exhibit the perovskite structure. Because of low solubility, an impure $SrCrO_4$ phase was observed (JCPDF card 73-1082) for samples calcined below 1200 °C [14,17,20,26]. For samples calcined at 1200 °C, $SrCrO_4$ dissolved into the perovskite [30] and a pure phase of perovskite powders remained. Notably, when higher calcination temperatures were used, less $SrCrO_4$ was detected (estimated from the peak intensities of $SrCrO_4$ in Fig. 1), which

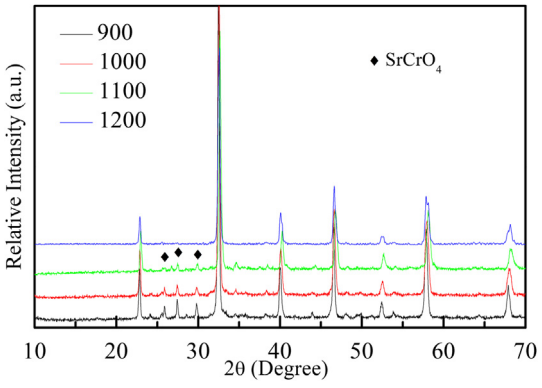

Fig. 1. XRD patterns of Fe 0.5 from powders calcined from 900 °C to 1200 °C.

indicates that more $SrCrO_4$ was dissolved in the perovskite. Therefore, single-phase perovskites of $La_{0.8}Sr_{0.2}Cr_{1-x}Fe_xO_{3-\delta}$ ($x = 0.1$, 0.2, 0.3, 0.4, and 0.5) can only be obtained by calcination at temperatures above 1200 °C.

The refined lattice parameters, crystal symmetries and calculated unit cell volumes of $La_{0.8}Sr_{0.2}Cr_{1-x}Fe_xO_{3-\delta}$ specimens ($x = 0.1$, 0.2, 0.3, 0.4, and 0.5) using 1200 °C calcined powders are systematically presented in Table 1. The lattice parameters and cell volumes increased with increasing Fe-doping levels, which is attributed to the larger cation radii of Fe^{3+} (0.645 Å) compared to Cr^{3+} (0.615 Å). Moreover, the crystal systems of Fe 0.1 to Fe 0.3 were characterised as having rhombohedral symmetry and belonging to the *R*3-*c* (167) space group, whereas Fe 0.4 and Fe 0.5 exhibited an orthorhombic structure with space group *Pbnm* (62), which is consistent with Tao's results [22]. Generally, $LaCrO_3$-type perovskite has two phases with orthorhombic and rhombohedral symmetries. It is reported that the structure of $La_{0.8}Sr_{0.2}CrO_3$ is rhombohedral [12], whereas $La_{0.8}Sr_{0.2}FeO_3$ exhibits an orthorhombic structure [27] at room temperature. Therefore, Fe-doping tends to promote the phase transition from rhombohedral to orthorhombic symmetry.

3.2. Chemical stability

To investigate the phase stability of $La_{0.8}Sr_{0.2}Cr_{1-x}Fe_xO_{3-\delta}$ perovskites in a reducing atmosphere, powders calcined at 1200 °C were exposed to wet H_2 at 900 °C for 6 h. Fig. 2 shows the XRD patterns as a function of Fe-doping level. After reduction, no phase segregation or decomposition product was observed. This suggests that the $La_{0.8}Sr_{0.2}Cr_{1-x}Fe_xO_{3-\delta}$ perovskites ($x = 0.1$, 0.2, 0.3, 0.4, and 0.5) are chemically stable under SOFC operating conditions, which is also consistent with Tao's results [22]. Fig. 3 shows the XRD patterns of the original and reduced specimens. The Fe 0.5 specimens are shown as representative results; the other compositions exhibited similar characteristics. No apparent peak shift was detected.

3.3. Sintering behaviour and a modified liquid-phase-assisted sintering mechanism

To investigate the densities and electrical conductivities of the samples, the 1200 °C calcined powders were pressed into rectangular bars at 250 MPa and sintered in air at 1400 °C for 4 h. Unfortunately, and as expected, all the samples were porous, as shown in Fig. 4 (Fe 0.5 is an example). A porosity of approximately 20–30% was estimated using SEM. Because of evaporation of chromium species and difficulty of diffusion, the densification of the materials was restricted at this temperature. Dense compounds were required to evaluate the thermal expansion and electrical conductivity. For this reason, the powder calcined at 1200 °C was not characterised further.

It has previously been mentioned that sintering Sr-doped lanthanum chromite perovskites results in an ex-solution of low melting $SrCrO_4$ [12,28,29] and that the liquid phase assists in densifying the perovskite. This is known as the "liquid-phase-assisted sintering mechanism" [29–31]. Thus, the degree of densification is associated with the amount of liquid phase [32]. Powders that were calcined at 1200 °C did not have a sufficient density, which may be attributed to the poor sintering activity and an insufficient amount of liquid phase. After considering all of the powders and adding sintering aids to improve the sinterability of doped lanthanum chromite powders, the powders calcined at 1000 °C were used for further studies in this work.

Table 1
Lattice parameters, cell volumes, and crystal symmetries of $La_{0.8}Sr_{0.2}Cr_{1-x}Fe_xO_{3-\delta}$ specimens.

Compositions	Lattice parameters			Space group	V (Å^3)	Z
	a (Å)	b (Å)	c (Å)			
Fe 0.1	5.52162	5.52162	5.52162	Rhombohedral	168.34	3
Fe 0.2	5.53294	5.53294	5.53294	Rhombohedral	169.38	3
Fe 0.3	5.54918	5.54918	5.54918	Rhombohedral	170.87	3
Fe 0.4	5.52572	5.55775	7.84079	Orthorhombic	240.80	4
Fe 0.5	5.53504	5.56535	7.82791	Orthorhombic	241.13	4

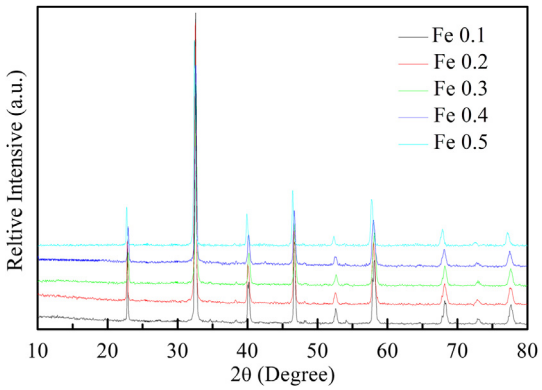

Fig. 2. XRD patterns of $La_{0.8}Sr_{0.2}Cr_{1-x}Fe_xO_{3-\delta}$ specimens after exposure to wet H_2 at 900 °C for 6 h.

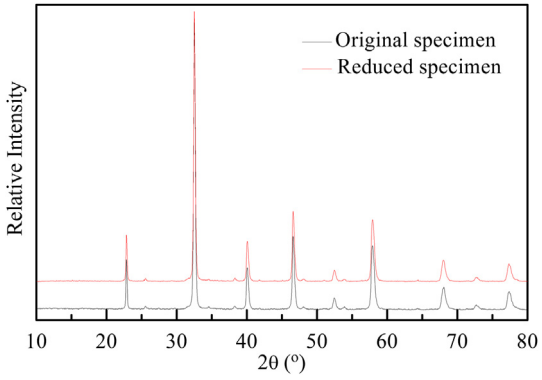

Fig. 3. XRD patterns of $La_{0.8}Sr_{0.2}Cr_{0.5}Fe_{0.5}O_{3-\delta}$ specimens before and after exposure to wet H_2 at 900 °C for 6 h.

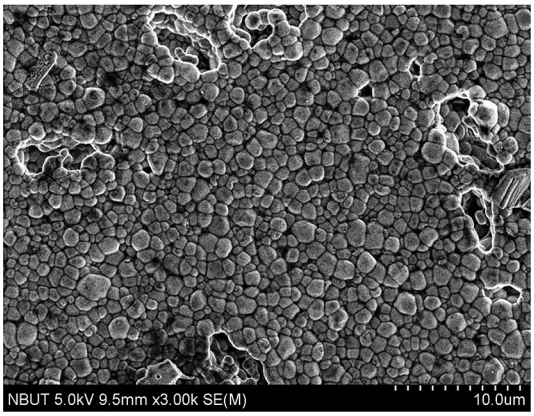

Fig. 4. SEM micrograph of Fe 0.5 sintered at 1400 °C for 4 h from powders calcined at 1200 °C.

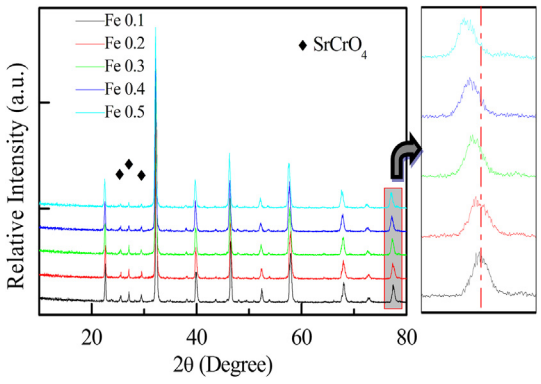

Fig. 5. XRD patterns of powders calcined at 1000 °C from $La_{0.8}Sr_{0.2}Cr_{1-x}Fe_xO_{3-\delta}$ specimens.

Fig. 5 shows the XRD patterns of $La_{0.8}Sr_{0.2}Cr_{1-x}Fe_xO_{3-\delta}$ ($x = 0.1$, 0.2, 0.3, 0.4, and 0.5) powder specimens, which were calcined at 1000 °C. The peaks of the XRD pattern gradually shift to lower angles (partly enlarged inset of Fig. 5) with increasing Fe-doping levels. This shift is indicative of an expansion in the unit cell with Fe-doping levels because the cation radii of Fe^{3+} is larger than Cr^{3+}, which is consistent with data in Table 1. Notably, all of the samples showed a minor phase of $SrCrO_4$, and the amount of $SrCrO_4$ decreased with Fe-doping levels. Using the reference intensity ratio method, the percentage of $SrCrO_4$ in Fe 0.1, Fe 0.2, Fe 0.3, Fe 0.4 and Fe 0.5 was calculated to be 5.8%, 4.9%, 3.8%, 3.2% and 2.7% (by mol), respectively [33], which suggests that $SrCrO_4$ functions as a sintering aid.

The 1000 °C calcined powders were pressed into rectangular bars at 250 MPa and sintered in air at 1400 °C for 4 h, similar to the procedure that was performed for the 1200 °C calcined powders. The bulk densities of the rectangular bars were measured using the Archimedes method, and the results are shown in Fig. 6. The relative densities of Fe 0.1, Fe 0.2, Fe 0.3, Fe 0.4 and Fe 0.5 were calculated to be 83.9%, 85.1%, 88.1%, 94.6% and 96.6%, respectively, which are significantly higher than the densities of the 1200 °C powders. Furthermore, the densities of Fe 0.4 and Fe 0.5 are higher than the value accepted (94%) for ceramic interconnects.

Fig. 7 and Fig. 8 show micrographs of the top surface and cross-section of rectangular bars sintered at 1400 °C using 1000 °C calcined powders, respectively. For Fe 0.1 (Fig 7 a) and Fe 0.2 (Fig 7 b), the surfaces are uneven and covered with several wrinkles, which represent traces of the melted liquid phase. However, excess liquid phase during sintering may cause shape distortion, as shown in Fig 8 a and b [32]. Additionally, the liquid phase may also migrate

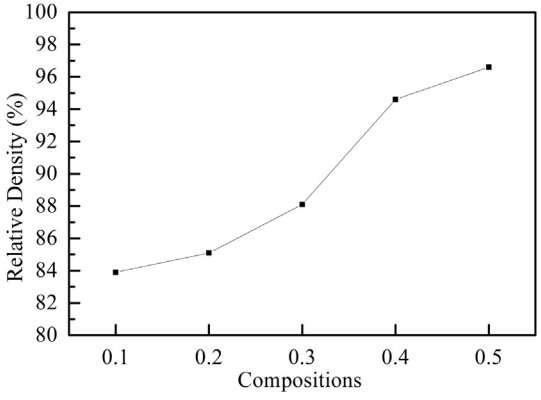

Fig. 6. Variations in the relative density of $La_{0.8}Sr_{0.2}Cr_{1-x}Fe_xO_{3-\delta}$ as a function of Fe-doping level.

to the anode interface during interconnect fabrication, which is not optimal.

Fe 0.3 (Figs 7 c and 8 c) exhibits similar characteristics to Fe 0.4 (Figs 7 d and 8 d), with the exception that Fe 0.3 has more pores. Micrographs of the top of the material show a more flat surface compared to Fe 0.1 and Fe 0.2. Notably, as the grains coalesced, liquid was expelled from the grain boundaries and spread into a uniform layer along the grain boundaries. This layer covered the grain boundaries and joined neighbouring particles, which significantly contributed to densification, as shown in Fig 7 f with additional details. A similar phenomenon was recently discovered by Sarıboğaet al [33]. To investigate the grain boundary conditions, we performed SEM–EDS mapping on the top surface of sample Fe 0.4. As shown in Fig. 9, La migrated to the grain boundary and excess La, Cr and O was visible. However, the grain boundaries also contained Sr-poor and Fe-poor regions. These results suggest that diffusion or redistribution of the liquid phase may occur during sintering. For example, with the disappearance of the liquid $SrCrO_4$ phase, the appearance of another phase is observed, such as lanthanum-rich La_2CrO_6 [31]. However, a detailed sintering mechanism for temperatures above 1200 °C requires further study.

Fe 0.5 (Figs 7 e and 8e) illustrates the "liquid-phase-assisted sintering mechanism". A relative density of 96.6% was calculated for Fe 0.5, and the smooth surface indicates that no liquid was formed on the surface during the sintering process. The precise formation of the liquid phase, which completely dissolved into the chromite, allowed neighbouring particles to merge during sintering [32]. This resulted in a homogenised and dense bulk material with only a few closed pores on the top surface of the bulk that was not gas permeable. Fig 8f shows a high magnification view of Fe 0.5, which consists of closely compacted fine grains with an average size of 1–2 μm and clear grain boundaries that exhibit perfectly straight grain growth. Based on these results, Fe 0.5 is the optimal material for SOFC interconnects among the $La_{0.8}Sr_{0.2}Cr_{1-x}Fe_xO_{3-\delta}$ ($x = 0.1$, 0.2, 0.3, 0.4, and 0.5) specimens.

During sintering of 1000 °C calcined powders at 1400 °C, the liquid phase should consist of the following two parts:

(1) Residual $SrCrO_4$ in the 1000 °C calcined powders that melted during sintering (similar to the sintering aids)
(2) The appearance of a lanthanum-rich phase at temperatures above 1200 °C.

As previously mentioned, residual $SrCrO_4$ decreased with Fe-doping levels (Fig. 5), which explains the phenomenon observed in Figs. 7 and 8. Taking the XRD results and Fig. 9 into consideration, the liquid $SrCrO_4$ phase contributed to densification at temperatures below 1200 °C, whereas the liquid lanthanum-rich phase played a more significant role at temperatures between 1200 °C and 1400 °C. The densification mechanism is unique and interesting. Neither the traditional "liquid-phase-assisted sintering mechanism" nor the method of adding other sintering aids was implemented; therefore, maybe "a modified liquid-phase-assisted sintering mechanism" can be developed. In summary, optimising the proper amount of liquid phase during liquid-phase-assisted sintering is a highly effective way to promote the densification of doped lanthanum chromites.

3.4. Thermal expansion and phase transition

The thermal expansions and electrical conductivities were evaluated using the rectangular bars sintered at 1400 °C using the 1000 °C calcined powders.

Fig. 10 (the solid line) illustrates the linear thermal expansion curves in the temperature range of 25–1000 °C for

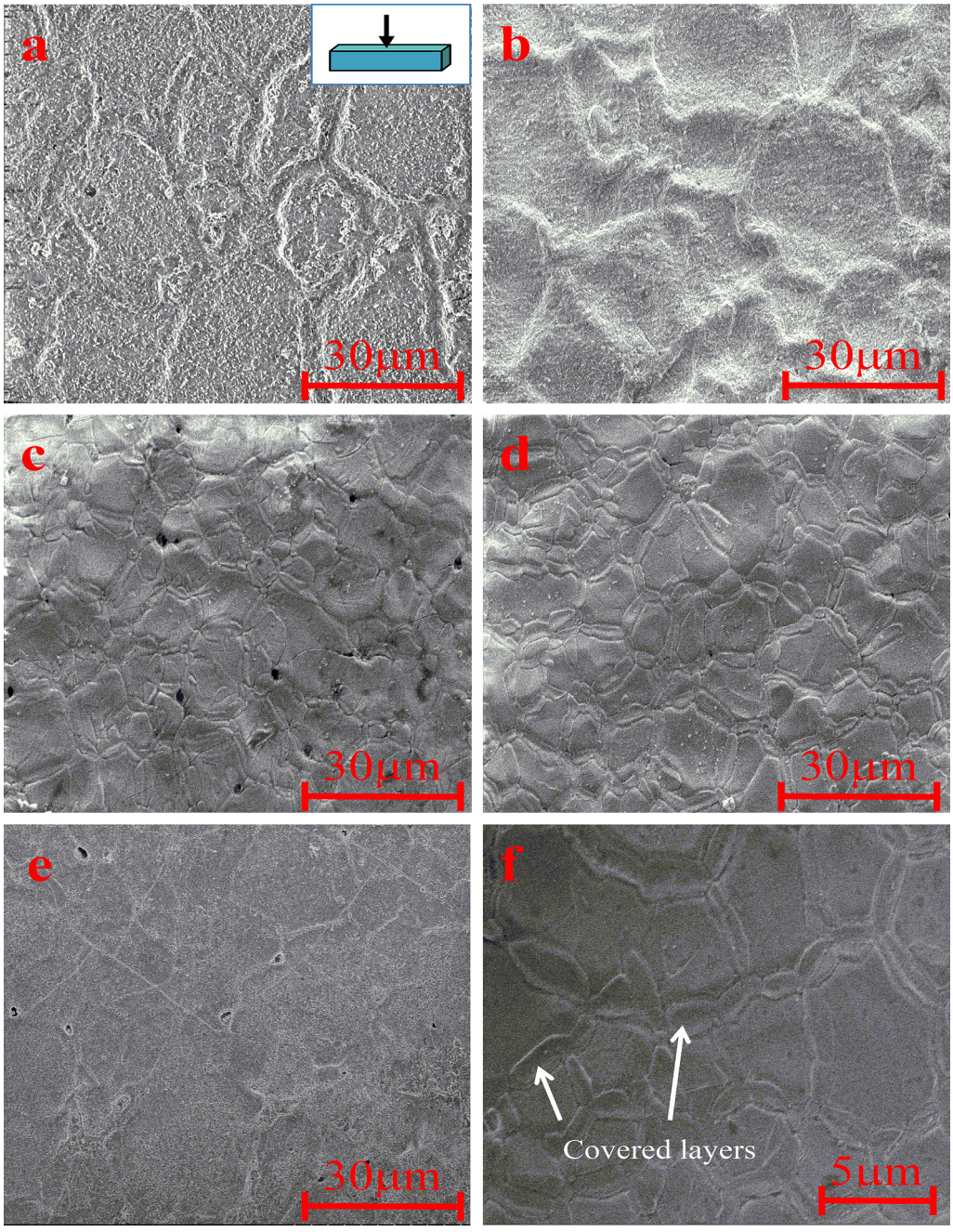

Fig. 7. Top surface micrographs of specimens sintered at 1400 °C for 4 h from 1000 °C calcined powders: (a) Fe 0.1, (b) Fe 0.2, (c) Fe 0.3, (d) Fe 0.4, (e) Fe 0.5, and (f) a high magnification view of Fe 0.4.

$La_{0.8}Sr_{0.2}Cr_{1-x}Fe_xO_{3-\delta}$ ($x = 0.1$, 0.2, 0.3, 0.4, and 0.5) specimens and YSZ (8 mol % Y_2O_3-stabilised ZrO_2). The curves nearly overlap, and the average thermal expansion coefficients of Fe 0.1, Fe 0.2, Fe 0.3, Fe 0.4 and Fe 0.5, were determined to be 10.8840×10^{-6}, 11.0293×10^{-6}, 10.9972×10^{-6}, 11.1184×10^{-6} and 11.4711×10^{-6} K^{-1} respectively. These values are similar to the average thermal expansion coefficient of 8 mol% YSZ (10.9455×10^{-6} K^{-1}) obtained in the same temperature range, as shown in Fig. 11. The TECs of $La_{0.8}Sr_{0.2}Cr_{1-x}Fe_xO_{3-\delta}$ series and YSZ are similar. Only the TEC of Fe 0.5 is slightly higher (4.8%) than the TEC of YSZ. The results of the current study indicate that Fe-doping has little effect on the TECs of lanthanum strontium chromites; average thermal expansion coefficients are nearly independent of x, which is consistent with Lü's results [24]. Thus, the $La_{0.8}Sr_{0.2}Cr_{1-x}Fe_xO_{3-\delta}$ series may be compatible with other cell components.

Stoichiometric and acceptor-doped lanthanum chromites typically experience a phase transition from orthorhombic to rhombohedral symmetry at 250–300 °C upon heating [34], as shown in Fig. 10. The thermal expansion curves of Fe 0.4 and Fe 0.5 were processed using a differential method (dashed line) to provide physical-TEC curves and more clearly present the phase transition phenomena. Structural phase transitions caused non-linear thermal expansion to occur at 112.5 °C for Fe 0.4 and 168.6 °C for Fe 0.5, respectively. However, this was not observed from Fe 0.1 to Fe 0.3, which further supports the phase structures listed in Table 1 by

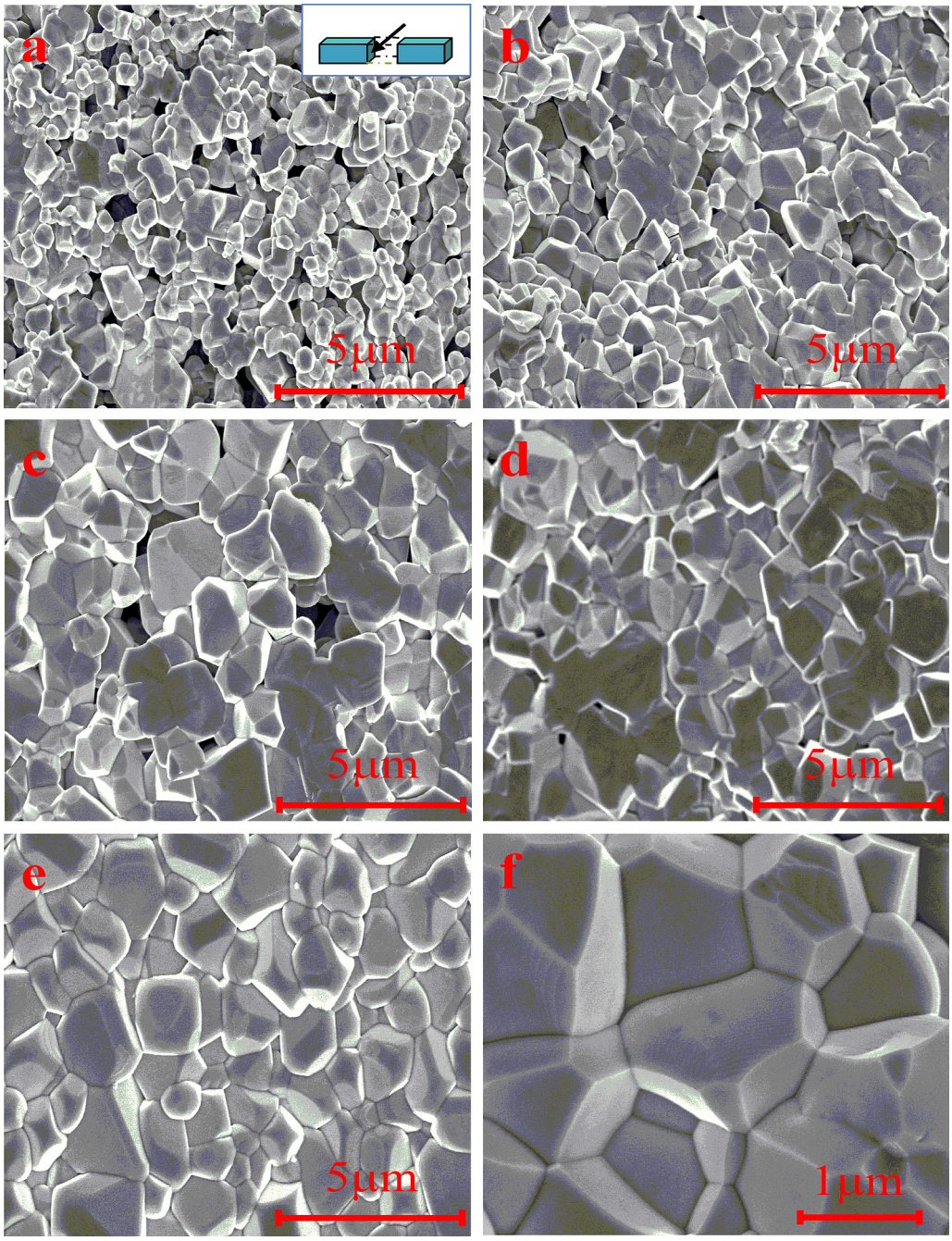

Fig. 8. Cross-sectional micrographs of specimens sintered at 1400 °C for 4 h from 1000 °C calcined powders: (a) Fe 0.1, (b) Fe 0.2, (c) Fe 0.3, (d) Fe 0.4, (e) Fe 0.5, and (f) a high magnification view of Fe 0.5.

XRD refinement. Generally, the phase transition occurring at 150 °C may have little effect on SOFC components. Because their TECs are comparable, relative thermal expansion was neglected.

3.5. Electrical conductivity

Electrical conductivity in air was measured using a four-probe DC method in the temperature range 650–850 °C. Fig. 12 shows the Arrhenius plots for the electrical conductivities in air of $La_{0.8}Sr_{0.2}Cr_{1-x}Fe_xO_{3-\delta}$ ($x = 0.1, 0.2, 0.3, 0.4$, and 0.5) specimens. The plots of log (σT) versus $1000/T^{-1}$ are nearly linear, which is consistent with the small polaron conduction mechanism [35]:

$$\sigma = \frac{C}{T}\exp\left(-\frac{E_a}{K_B T}\right)$$

where E_a is the activation energy, k_B is the Boltzmann constant, and T is the absolute temperature. For all of the compositions, the conductivity increased with Fe-doping levels, and the conductivity of $La_{0.8}Sr_{0.2}Cr_{0.5}Fe_{0.5}O_{3-\delta}$ was calculated to be 21.88 S cm^{-1} in air and 6.45 S cm^{-1} in 5% H_2/Ar at 800 °C [36], respectively. The

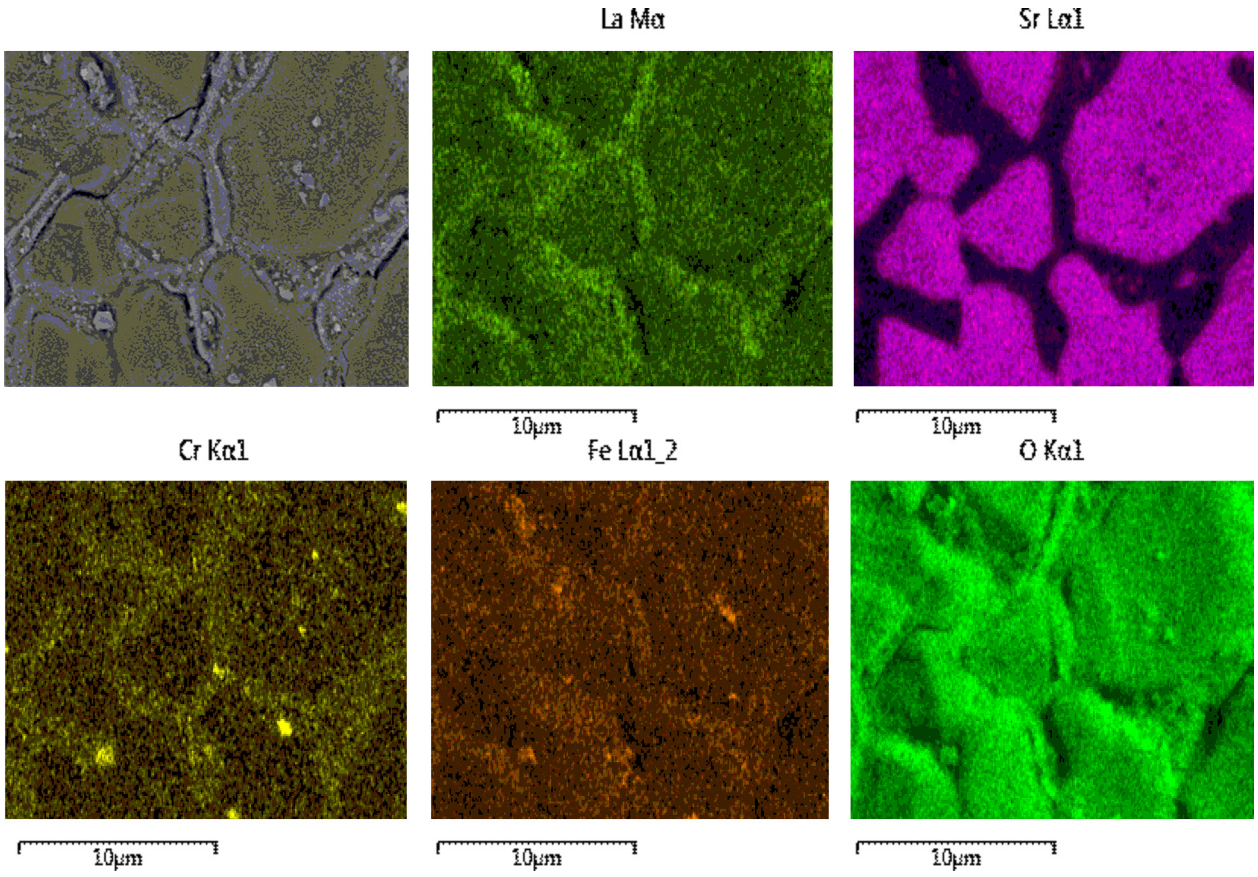

Fig. 9. The energy dispersive X-ray elemental mapping of La, Sr, Cr, Fe and the overall distribution on the top surface of the Fe 0.4 sample.

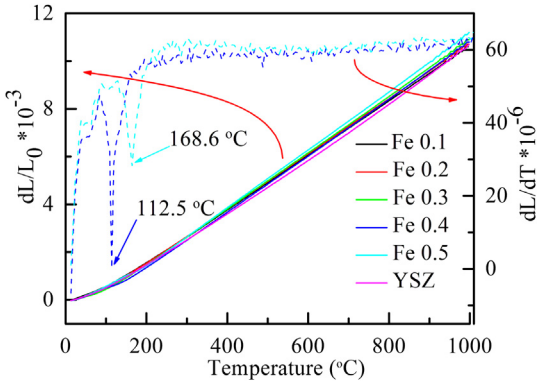

Fig. 10. Linear thermal expansion curves for $La_{0.8}Sr_{0.2}Cr_{1-x}Fe_xO_{3-\delta}$ and YSZ.

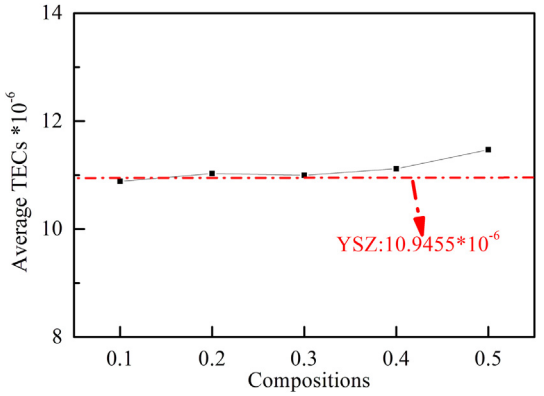

Fig. 11. The average thermal expansion coefficients of $La_{0.8}Sr_{0.2}Cr_{1-x}Fe_xO_{3-\delta}$ compared to YSZ.

activation energy obtained from the slope of Fig. 10 was 0.282 eV for Fe 0.5, which is sufficient for SOFC interconnects.

4. Conclusions

Fe-doped lanthanum strontium chromites, i.e., $La_{0.8}Sr_{0.2}Cr_{1-x}Fe_xO_{3-\delta}$ (x = 0.1, 0.2, 0.3, 0.4, 0.5), were synthesised on B-sites and evaluated as potential interconnect materials for SOFCs. A modified liquid-phase-assisted sintering mechanism was employed to improve the sinterability of $La_{0.8}Sr_{0.2}Cr_{1-x}Fe_xO_{3-\delta}$ powders. A distinct transient liquid phase was formed during the sintering process that spread into a uniform layer along the free-surface and covered the grain boundaries. This enhanced the densification of samples from powders calcined at 1000 °C. Relative

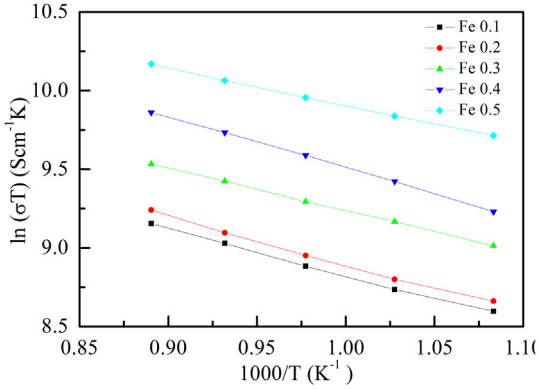

Fig. 12. Arrhenius plots for the electrical conductivities of the $La_{0.8}Sr_{0.2}Cr_{1-x}Fe_xO_{3-\delta}$ series in air.

densities of 94.6% and 96.6% were successfully obtained for Fe 0.4 and Fe 0.5, respectively. Additionally, it was determined that electrical conductivity increased with Fe-doping levels and that the conductivity of $La_{0.8}Sr_{0.2}Cr_{0.5}Fe_{0.5}O_{3-\delta}$ is 21.88 S cm^{-1} in air and 6.45 S cm^{-1} in 5% H_2/Ar at 800 °C. XRD measurements indicated that no iron or other decomposition products in the reduced samples were detected after the samples were heated at 900 °C for 6 h under a flow of H_2, which indicates that $La_{0.8}Sr_{0.2}Cr_{1-x}Fe_xO_{3-\delta}$ is redox-stable. Therefore, Fe 0.5 is a promising alternative interconnect for solid oxide fuel cells. Furthermore, using the proper amount of liquid phase during liquid-phase-assisted sintering is highly effective in promoting the densification of doped lanthanum chromites, which is advantageous toward the development of SOFC separator materials.

Acknowledgements

This work was financially supported by grants from the National Science Foundation of Jiangsu Province (BK2011006), PAPD, Fundamental Research Funds (No. 2013XK05) for the Central Universities, the National Natural Science Foundation of China (51071169) and Jiangsu Ordinary University Graduate Innovative Research Programs.

References

[1] N.Q. Minh, J. Am. Ceram. Soc. 76 (1993) 563–588.
[2] N.Q. Minh, Solid State Ionics 174 (2004) 271–277.
[3] B.C.H. Steele, A. Heinzel, Nature 414 (2001) 345–352.
[4] L. Zhou, M. Cheng, B. Yi, Y. Dong, Y. Cong, W. Yang, Electrochim. Acta 53 (2008) 5195–5198.
[5] R. Liu, C. Zhao, J. Li, S. Wang, Z. Wen, T. Wen, J. Power Sources 195 (2010) 541–545.
[6] T.H. Lim, J.L. Park, S.B. Lee, S.J. Park, R.H. Song, D.R. Shin, Int. J. Hydrogen Energy 35 (2010) 9687–9692.
[7] U.B. Pal, Solid State Ionics 52 (1992) 227–233.
[8] B. Lin, S. Wang, X. Liu, G. Meng, J. Alloys Compd. 490 (1–2) (2010) 214–222.
[9] C. Yamaqata, S.R.H. Mello-Castanho, Mater. Sci. Forum 660–661 (2010) 971–976.
[10] Y.P. Fu, H.C. Wang, S.H. Hu, K.W. Tay, Ceram. Int. 37 (7) (2011) 2127–2134.
[11] N.E. Cipollini, B.L. Wu, S. Haig, J. Yamanis, U.S. Patent 5169811, 1992.
[12] M. Mori, Y. Hiei, N.M. Sammes, Solid State Ionics 135 (2000) 743–748.
[13] M. Mori, T. Yamamoto, T. Ichikawa, Y. Takeda, Solid State Ionics 148 (2002) 93–101.
[14] N. Sakai, T. Kawada, T. Yokokawa, M. Dokiya, T. Iwata, J. Mater. Sci. 25 (1990) 4531–4534.
[15] J.D. Carter, M.M. Nasrallah, H.U. Anderson, J. Mater. Sci. 31 (1996) 157–163.
[16] S. Wang, B. Lin, K. Xie, Y. Dong, X. Liu, G. Meng, J. Alloys Compd. 468 (2009) 499–504.
[17] N. Sakai, H. Yokokawa, T. Horita, K. Yamaji, Int. J. Appl. Ceram. Technol. 1 (2004) 23–30.
[18] J.D. Carter, C.C. Appel, M. Mogensen, J. Solid State Chem. 122 (1996) 407–415.
[19] I. Yasuda, T. Hikita, J. Mater. Sci. 29 (1994) 2801–2805.
[20] T.R. Armstrong, J.W. Stevenson, L.R. Pederson, P.E. Raney, J. Electrochem. Soc. 143 (1996) 2919–2925.
[21] K.J. Yoon, J.W. Stevenson, O.A. Marina, J. Power Sources 196 (20) (2011) 8531–8538.
[22] S. Tao, J.T.S. Irvine, Chem. Mater. 16 (5) (2004) 4116–4121.
[23] J. Liu, T. Liu, W. Wang, J. Gao, C. Chen, J. Memb. Sci. 389 (2012) 435–440.
[24] M.F. Lü, E.V. Tsipis, J.C. Waerenborgh, A.A. Yaremchenko, V.A. Kolotygin, S. Bredikhin, V.V. Kharton, J. Power Sources 206 (2012) 59–69.
[25] M. Mori, N.M. Sammes, Solid State Ionics 146 (2002) 301–312.
[26] S.P. Simner, J.S. Hardy, J.W. Stevenson, T.R. Armstrong, Solid State Ionics 128 (2000) 53–63.
[27] S.E. Dann, D.B. Currie, M.T. Weller, J. Solid State Chem. 109 (1994) 134–144.
[28] R. Koc, H.U. Anderson, J. Eur. Ceram. Soc. 9 (1992) 285–292.
[29] N. Sakai, T. Kawada, H. Yokokawa, M. Dokiya, I. Kojima, J. Am. Ceram. Soc. 76 (1993) 609–616.
[30] L.A. Chick, J. Liu, J.W. Stevenson, T.R. Armstrong, D.E. McCready, G.D. Maupin, G.W. Coffey, C.A. Coyle, J. Am. Ceram. Soc. 80 (1997) 2109–2120.
[31] S.P. Simner, J.S. Hardy, J.W. Stevenson, T.R. Armstrong, J. Mater. Sci. 34 (1999) 5721–5732.
[32] R.M. German, S. Farooq, C.M. Kipphut, Mater. Sci. Eng. A 105/106 (1988) 215–224.
[33] V. Sarıboğa, H. Özdemir, M.A.F. Öksüzömer, J. Eur. Ceram. Soc. 33 (2013) 1435–1446.
[34] K. Oikawa, T. Kamiyama, T. Hashimoto, Y. Shimojyo, Y. Morii, J. Solid State Chem. 154 (2000) 524–529.
[35] D. Pkarim, A.T. Aldred, Phys. Rev. B 20 (1979) 2255–2263.
[36] N. Danilovic, A. Vincent, J. Luo, K.T. Chuang, R. Hui, A.R. Sanger, Chem. Mater. 22 (2010) 957–965.